Preparation and Photocatalytic Activity of TiO₂-Wrapped Cotton Nanofiber Composite Catalysts

Liruhua Zhang,[a] Junmin Wan,[a,b,*] Zhiwen Hu,[b] and Wenbin Jiang [b]

A novel TiO₂-wrapped nanofiber composite catalyst, which possessed a unique porous structure and mixed crystalline phase, was prepared by the combination of superficial sol–gel and post-calcination processes. By means of the superficial sol–gel process, TiO₂ layers were deposited on the surface of each nanofiber-like cellulose fiber, and then the TiO₂-wrapped nanofiber composite catalysts were calcined at different temperatures under a nitrogen atmosphere. With temperature increasing, the original cotton nanofiber composites were converted into porous carbon nanofiber catalysts wrapped by a TiO₂ mixed crystalline phase, which was accompanied by a crystal transformation. The photocatalytic activity of the new catalysts was evaluated by the degradation of methylene blue (MB) under ultraviolet (UV) irradiation. The results demonstrated that the new catalysts had good photocatalytic ability, and the TNC-700 catalyst showed a superior photocatalytic ability compared with the other catalysts; the new catalysts had a unique porous structure, high specific surface area, and mixed crystalline phase. Additionally, the synergistic photocatalytic effect of the TiO₂ and activated carbon nanofiber resulted in the efficient degradation of organic pollutants in water or air.

Contact information: a: National Engineering Lab of Textile Fiber Materials & Processing Technology, Zhejiang Sci-Tech University, Hangzhou 310018, PR China; b: State Key Laboratory of Advanced Textiles Materials and Manufacture Technology, MOE, Zhejiang Sci-Tech University, Hangzhou 310018, PR China; *Corresponding authors: wwjm2001@126.com

INTRODUCTION

Organic/inorganic (hybrid) nanocomposites have attracted increasing attention because of their remarkable synergistic effects and applications in different fields (Alexandre and Dubois 2000; Sinha Ray and Okamoto 2003; Jia *et al.* 2012; Stoica-Guzun *et al.* 2013). With the strong awareness of recycled, sustainable, and biodegradable polymeric materials, biopolymers are considered to be prime material for nanocomposites. Silk (Foo *et al.* 2006; Kharlampieva *et al.* 2010), cellulose (Eichhorn *et al.* 2010; Klemm *et al.* 2011; Bi *et al.* 2013), chitin (Alonso and Belamie 2010; Ifuku *et al.* 2010), collagen (Marandi *et al.* 2013), starch (Matsui *et al.* 2004), and alginates (Rhim *et al.* 2006) have all been utilized to prepare organic/inorganic hybrid composites. Different methods have been utilized to fabricate the hybrid materials, which combined the biomass substances with inorganic materials. For example, Cook and Timms designed an exact replication of biological structure by using chemical vapor deposition (CVD) of silica (Cook and Timms 2003). Atomic layer deposition (ALD) was used for the preparation of photocatalytic TiO₂/cellulose composites in nanometer-level replication of cellulosic substances (Kemell *et al.* 2005).

With regard to these biopolymers, nanocrystalline cellulose (NCC), which is nanosized cellulose fiber, has a number of fascinating characteristics, such as containing a large number of active hydroxyl groups on its surface, environmentally friendly nature, low cost, nanoscale dimension, and unique optical properties and utilities (de Souza Lima *et al.* 2004; Beck-Candanedo *et al.* 2005; Klemm *et al.* 2005; Foo *et al.* 2006; Klemm *et al.* 2006; Thakur and Thakur 2014; Thakur and Voicu 2016). Recently, to explore multifunctional nanocellulose hybrid composites, many different nanocellulose-inorganic hybrid composite materials have been prepared for applications in various fields. Nanocellulose-silver hybrids have been prepared as potential antibacterial agents (Díez *et al.* 2011). Homogeneous hybrids from NCC and spherical nanoparticles of amorphous calcium carbonate (ACC) were obtained by a simple chemical approach (Gebauer *et al.* 2011). Titanium dioxide (TiO_2) coated nanocellulose aerogels showed photoswitchable hydrophobicity and photooxidative decomposition from a chemical vapor deposition (CVD) approach (Kettunen *et al.* 2011). Nanocellulose aerogel with a hydrophobic and oleophilic coat was achieved by functionalizing the native cellulose nanofibrils with a nanoscopic layer of TiO_2 (Korhonen *et al.* 2011). Among these composites, as should be noted that nanocellulose-titania hybrid composite composites with well-defined structures could be acquired. Furthermore, carbonization of the natural cellulose substances under proper temperature and atmosphere could acquire unique nanostructured carbon materials because of the rigidity and thermal stability of the nanocrystalline cellulose.

TiO_2 is an ideal and stable photocatalyst, and it is capable of degrading organic molecules *via* electrons and holes formed under ultraviolet (UV) light irradiation. There is tremendous amount of interest for TiO_2 in photocatalytic applications because of the increasing demand for environmental remediation and energy conservation. TiO_2-based materials are promising photocatalysts that have many advantages, such as non-toxicity, low cost, good photocatalytic activity, and chemical stability (Khan *et al.* 2002; Zhang *et al.* 2008). Unfortunately, the low electrical conversion efficiency has caused serious challenges because of the narrow light-response range of UV (only about 3% to 5% of total sunlight) (Liu *et al.* 2008), and the electrons and holes can easily recombine before the electrons emigrate to the surface of the photocatalysts. Considerable efforts have been exerted to design a special structural material of TiO_2 to improve the photoelectric conversion efficiency. There are a number of possibilities for the synthesis of structural materials of TiO_2 by using biological macromolecules as carriers or composites. It is worth noting that titania-carbon composite materials, which possess synergistic effects from the TiO_2 and carbon, have a better photocatalytic performance than pure TiO_2 materials (Shanmugasundaram and Horst 2003; Yang and Tian 2015). Both the nanostructure and high surface area are very important for enhancing the photocatalytic efficiency of TiO_2. Many studies have been reported that cellulosic substances have been used as support template of titania films for developing the novel catalytic hybrids. However, the photocatalytic activity achieved was relatively poor due to some faulty structure or relatively low surface area of only 4 m^2g^{-1} (Kemell *et al.* 2005). To the best of our knowledge, there has been a lack of work to investigate the influence of the different calcination temperature for the fabrication of TiO_2/activated carbon fiber hybrids materials under the nitrogen atmosphere. Therefore, it is very important to investigate the optimum conditions of TiO_2 wrapped activated carbon fiber hybrids materials systematically. As shown in this paper, these issues can be solved.

In this paper, the mesoporous and nanorod-like TiO_2-wrapped nanofiber composite catalysts were acquired by a facile method, which could be applied for degradation of the wastewater. The morphology, crystalline phase, specific surface area, and chemical composition of the prepared photocatalysts were characterized by scanning electron microscopy (SEM), transmission electron microscopy (TEM), X-ray diffraction (XRD) analysis, Fourier transform infrared (FTIR) spectroscopy, thermogravimetric and differential thermal analysis (TG-DTA), Brunauer-Emmett-Teller (BET) method, and X-ray photoelectron spectroscopy (XPS). Additionally, the photocatalytic activity of the prepared photocatalysts was evaluated by degrading methylene blue (MB) solution under UV irradiation. The results showed that the photocatalytic activity of the new photocatalysts was improved because of its highly unique porous structure, mixed crystalline phase, and synergistic effect between TiO_2 and porous activated carbon nanofibres. Thus, the prepared photocatalysts could be used potentially to degrade organic pollutants in water or air.

EXPERIMENTAL

Preparation of NCC Cotton Fiber

All chemical reagents were of analytical grade and used without further purification. The NCC was prepared by sulfuric acid hydrolysis of CP20 cotton linters (Aladdin, China). First, the cotton fibers were washed with deionized water and dried at 60 °C. A 220-mL portion of 64% H_2SO_4 (109 mL of concentrated sulfuric acid with 111 mL of deionized water) was added to a round bottom flask and heated at 45 °C in a water bath for 1 h. A total of 20 g of cotton fiber was added to the round bottom flask, which was vigorously stirred at 45 °C for 45 min. The solution became white when the cotton paddle was completely dissolved, and then became pale yellow when heated at a constant temperature. The suspension was diluted 10-fold with deionized water, and the NCC-containing fraction was left in the bottom sediment over-night. The upper liquid phase was decanted. Afterwards, the NCC-rich phase was washed three times with deionized water and centrifuged at 8500 rpm. A finely dispersed NCC fiber thick solution was then obtained with a mass fraction of approximately 6 wt.%.

Synthesis of TiO_2-Wrapped Nanofiber Composite Catalysts

An appropriate amount of crystalline nanocellulose solution was added to 180 mL of absolute ethanol, and homogeneously dispersed solution A was obtained after ultrasonic treatment. Solution B was obtained by adding 6 mL of butyl titanate dropwise into 180 mL of absolute ethanol solution isolated from the air, and then stirred vigorously. Solution B was slowly poured into solution A, and the mixed solution was vigorously stirred for 30 min to obtain solution C. A mixed solution of absolute ethanol: water (1:10) was added into solution C. The final solution was continuously stirred for 24 h in the air. The TiO_2-wrapped nanofiber composites were collected by centrifugation, washed several times with deionized water and absolute ethanol, and air-dried at 60 °C for 3 h. The samples were divided and calcined at 500, 600, 700, 800, and 900 °C in a N_2 atmosphere for 2 h. The original TiO_2-wrapped nanofiber composites were coded as TNC, and the TiO_2-wrapped nanofiber composites that were calcined at 500, 600, 700, 800, and 900 °C in a N_2

atmosphere were coded as TNC-500, TNC-600, TNC-700, TNC-800, and TNC-900, respectively.

Characterization

The functional group changes of the samples at different calcination temperatures were determined using FTIR spectra, which were measured on a Nicolet Nexus spectrometer (Thermo Scientific, USA) with the samples embedded in KBr pellets. For the microsurface analysis, the samples were observed with SEM and TEM. A ZEISS SUPRA 40 scanning electron microscope (Zeiss, Germany) was used to obtain the images. TEM was carried out with a Tecnai G20 instrument (FEI, USA) operated at 100 kV. The samples were mixed in ethanol and then underwent supersonic oscillations for 10 min. Drops of the suspension were placed on carbon coated copper or silicon wafer grids for analysis after desiccation. The crystalline structures were characterized by XRD (miniflex600, Rigaku, Japan) using Ni-filtered Cu Kα radiation ($\lambda = 1.5406$Å) at 40 kV and 44 mA. The samples were scanned within the 2θ range of 10° to 80° at a scanning speed of 1°/min. The specific surface area (S_{BET}), pore volume (V_p), and crystal size of the samples were measured by the BET method at a relative pressure (p/p_0) ratio of 0.05 to 0.2 based on the N_2 adsorption at the liquid-nitrogen temperature using a Micro ASAP2460 unit (Micro, USA). To determine the thermal decomposition behavior of the samples, TG-DTA was performed at a heating rate of 10°C/min in air with a SHIMADZU-DTG60 thermogravimetric analyzer (Shimadzu, Japan). XPS (K-Alpha, Thermofisher Scientific Company, Thermo Scientific, USA) was performed to characterize the elemental composition of the prepared samples.

Evaluation of the Photocatalytic Activity

The photocatalytic activities of the samples were evaluated using MB as the target degradation molecule in a reactor under UV light irradiation. The irradiation source was a 1000 W mercury lamp ($\lambda < 400$ nm). The initial concentration of MB was 10 mg/L, and the MB solution was kept at 25 °C. The photocatalytic experiments were carried out without bubbling. The MB solution in the photoreactor was always open for air with magnetic stirring. The reaction was composed of 10 mg of catalyst and 30 mL of MB solution with an original concentration of 10 mg/L. Before turning the light on, the solution was stirred with a magnetic bar for 1 h to ensure the adsorption-desorption equilibrium between the dye and catalyst. A total of 4 mL of the suspension was analyzed at 0.5 h intervals by recording the dye absorption spectra.

RESULTS AND DISCUSSION

Synthesis Approach of the Composite Catalysts

The fabrication procedure of theTiO₂-wrapped nanofiber composite catalysts is schematically illustrated in Fig. 1. The TiO₂-wrapped nanofiber catalysts were fabricated with two steps. Firstly, pre-hydrolyzed butyl titanate (TBOT) was added to the aqueous suspension of cotton nanofiber, and then an opaque colloidal dispersion solution was acquired after continuous stirring. Finally, the samples were calcined at different temperatures under a nitrogen atmosphere (Fig. 1).
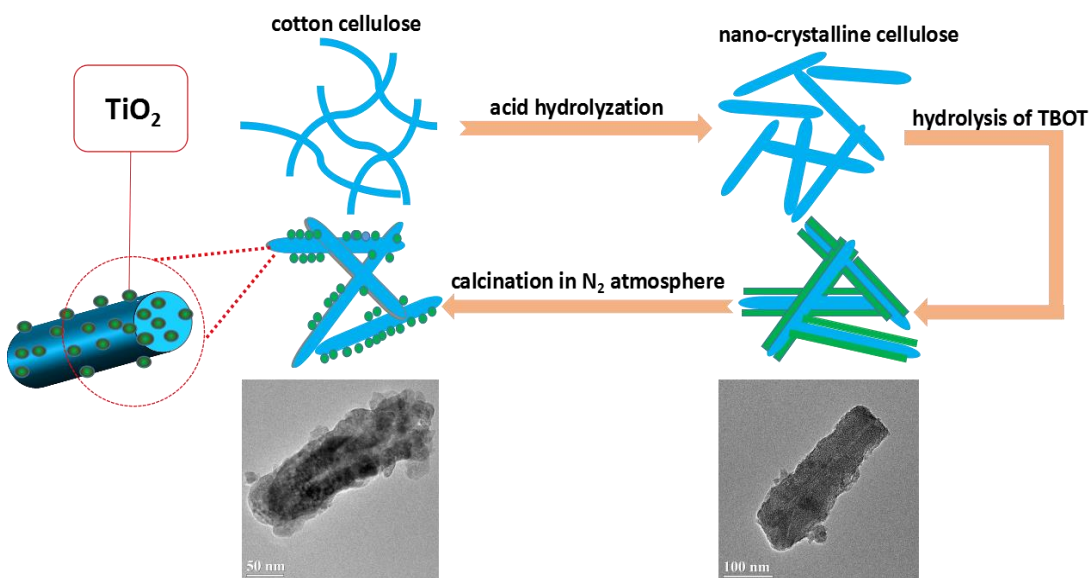
Fig. 1. Synthesis process of the TiO_2-wrapped nanofiber composite catalysts

FTIR Spectroscopy Analysis of the Composite Catalysts

The FTIR spectra of the TNC, TNC-500, TNC-600, TNC-700, TNC-800, and TNC-900 samples are shown in Fig. 2. All samples had strong bands at 400 to 900 cm^{-1}, which corresponded to Ti–O–Ti bridge stretching and Ti–O stretching modes. The strong broad band near 3436 and 1634 cm^{-1} appeared in Fig. 2 (a, b, c, and d), which were assigned to the stretching and deformation vibration of the hydroxyl groups present (C-OH and TiO_2-OH) in the surface of active carbon nanofiber and TiO_2 composite sample (Ao *et al.* 2008). The intensive band of OH-group asymmetrical and symmetrical stretching vibrations at 3436 cm^{-1} and H-O-H deformation vibration at 1634 cm^{-1} could confirm the large amount of water molecules. However, the OH-group vibration bands became much weaker with the increase of calcination temperatures (Chen *et al.* 2003; Bezrodna *et al.* 2004; Watson *et al.* 2004).
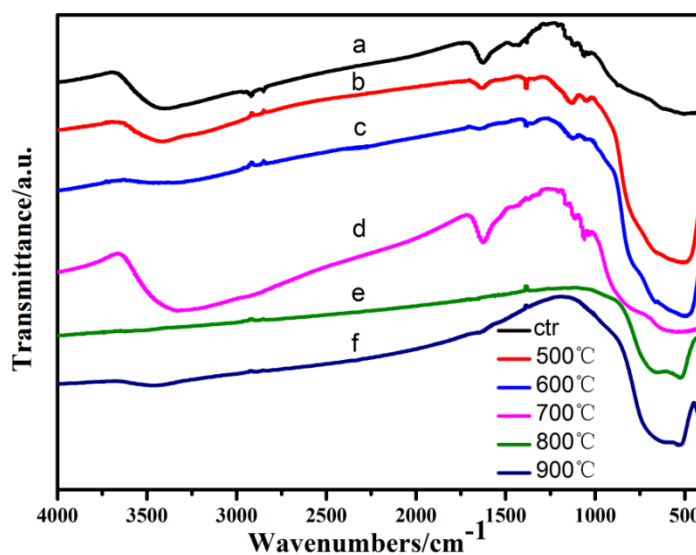

Fig. 2. FTIR spectra of the samples calcined at different temperatures

The aforementioned bands at 3436 and 1634 cm^{-1} were assigned to the bending vibration absorption of OH-group; both bands completely vanished when the calcination temperature increased above 700 °C. In other words, the spectra of the TNC-800 and TNC-900 samples did not show the two broad peaks (Jia *et al.* 2009). These results indicated that a mass of OH-group and absorbed water molecules in TNC-800 and TNC-900 had been removed with the rising of the temperature above 700°C. In some extent, the disappearance of both bands at 3436 and 1634 cm^{-1} of the TNC-800 and TNC-900 resulted in the reduction of the photocatalytic activities. The bands from the range of 1000 to 1400 cm^{-1} in the spectra of a, b, c, and d in Fig. 2 were caused by O-H bending vibration and C-OH stretching, which indicated the existence of many residual surface OH-group in these samples (Sun and Li 2004; Zhu *et al.* 2007). In the photocatalytic reaction, the surface OH-group, which can react with photogenerated holes on the surface of the catalyst, played a major role in enhancing the photocatalytic activity. Because the surface OH-group resulted in better charge transfer, the recombination of the electron-hole pairs was inhibited, and there were higher concentrations of hydroxyl radicals, which were vital oxidants for the photocatalytic reaction. Therefore, the surface area and pore volume were reduced during high temperature calcination (Table 1).

SEM and TEM Analysis of the Composite Catalysts

The morphological changes of the TiO$_2$-wrapped nanofiber composite catalysts calcined at different temperatures were analyzed by SEM and TEM, and the images are shown in Figs. 3 and 4, respectively.
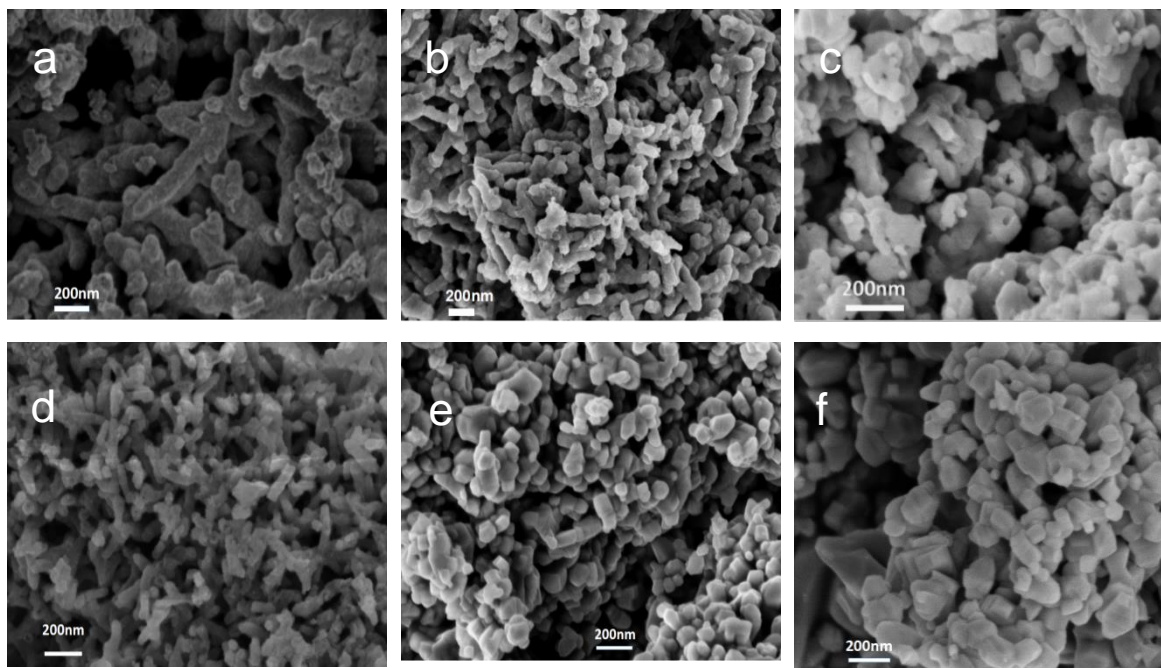

Fig. 3. SEM images of (a) TNC, (b) TNC-500, (c) TNC-600, (d) TNC-700, (e) TNC-800, and (f) TNC-900

The TiO$_2$-wrapped nanofiber composite catalysts showed a nanorod morphology with different pore volumes at different calcination temperatures. The image of the original

TiO$_2$-wrapped nanofiber composite catalyst (Fig. 3a) showed a nanofiber core-shell structure, which was further confirmed by the TEM (Fig. 4a). The TEM image of the original samples revealed that the coating of TiO$_2$ was uniform and dense on the surface. Figures 3 b, c, d, e, and f present the low magnification SEM images of the calcined products. The TNC-500 samples (Fig. 3b) showed some apparent changes in the morphology, and had more irregular nanopores. When the calcination temperature was increased up to 600 °C (TNC-600), more agglomerates of TiO$_2$-wrapped nanofiber composite catalysts were observed (Fig. 3c). The interaction effect between the small TiO$_2$ nanoparticles, which deposited on the surface of the nanofiber, might have caused agglomeration, and led to a decreased surface area (24.07 m²/g) compared with TNC-500 (48.46 m²/g), as shown in Table 1. The samples calcined at and below 700 °C remained nanorod-like in shape. For theTNC-800 and TNC-900 samples, only TiO$_2$ nanoparticles were observed because the high temperature degraded the nanocellulose.
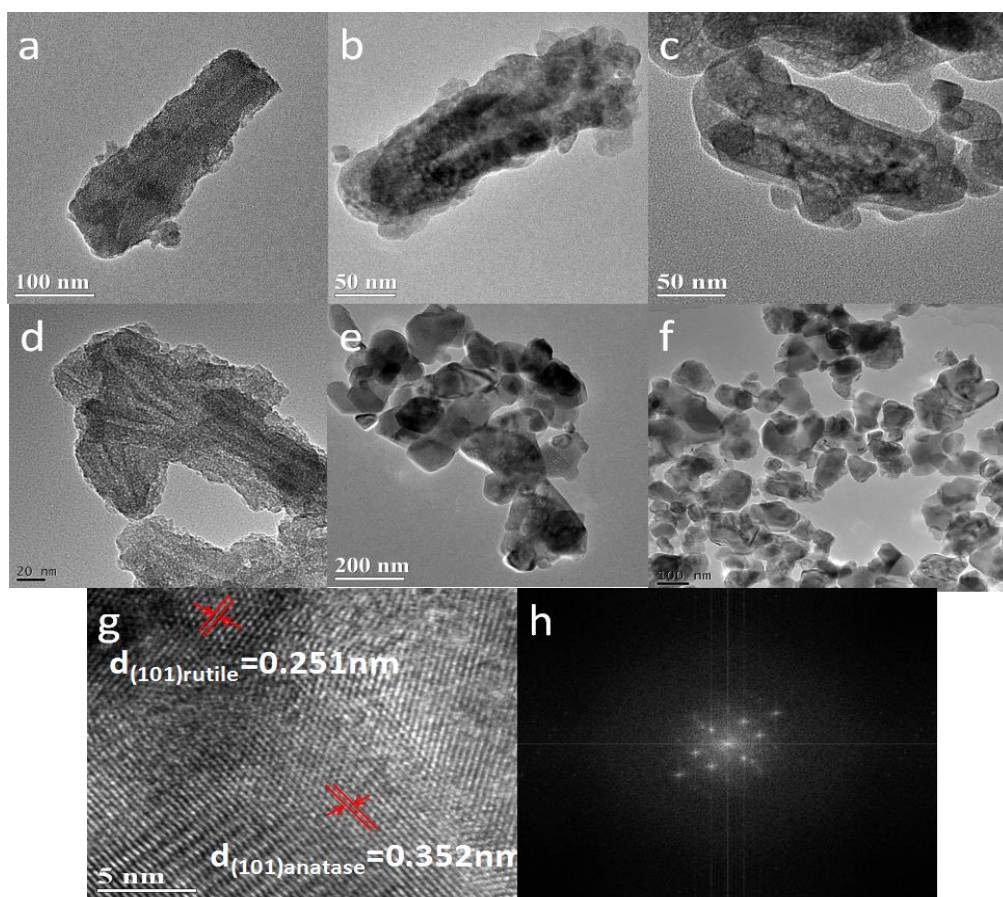

Fig. 4. TEM images of (a) TNC, (b) TNC-500, (c) TNC-600, (d) TNC-700, (e) TNC-800, and (f) TNC-900; (g) HRTEM of TNC-700; (h) the SAED pattern image of TNC-700

The TEM images showed much finer morphological changes and crystal structure of the calcined TNC samples. TNC-700 (Fig. 4d) showed a nanofiber-like morphology of TiO$_2$ with a porous structure, which led to an improvement of the pore volume (0.2083 cm^3/g). Additionally, the TiO$_2$ wrapped nanofibers mainly accumulated in the direction of the cotton cellulose nanofibers. The high resolution TEM (HRTEM) image of TNC-700 (Fig. 4g) showed an interplanar spacing (d) of 0.365 and 0.251 nm, which corresponded to

the (101) plane of the anatase and rutile phases, respectively. The selected area electron diffraction (SAED) pattern of TNC-700 (Fig. 4h) indicated that there were mixed polycrystalline phases, including anatase and rutile, which was in accordance with the results of the XRD patterns, as shown in Fig. 5. The crystalline phase structure of TiO_2 played an important role in the photoelectrochemical properties and photocatalytic activity. High crystallinity could diminish the recombination of the photogenerated charges and holes in the bulk and on the surface of the photocatalysts. So, high temperature calcination was a simple and effective approach to improve the crystallinity.

XRD Analysis of the Composite Catalysts

Figure 5 showed the XRD patterns of the samples calcined at different temperatures. There were no apparent diffraction peaks in the pure sample (Fig. 5 a). However, strong diffraction peaks were observed for the other calcination samples, which indicated the formation of new crystal structures at high temperatures. In Fig. 5 b, the diffraction peaks at 25.2°, 36.9°, 37.8°, 38.6°, 48.0°, 53.9°, and 55.1° were related to the diffractions of the (101), (103), (004), (112), (200), (105), and (211) planes of anatase TiO_2 (JCPDS No. 21-1272), respectively (Zhang *et al.* 1999; Zhang *et al.* 2000; Bae *et al.* 2009; Li and Zeng 2011). The crystalline phase of the calcined samples showed a slightly stronger diffractive intensity with the increase of temperature, *i.e.*, the higher temperature, then the stronger diffractive intensity. However, when the calcination temperature was 700 °C or higher, the diffraction features of rutile TiO_2 (JCPDS No. 21-1276) were observed (Fig. 3 d). Additionally, the TNC-800 and TNC-900 samples clearly showed the sharper diffractive peaks that are typical of rutile TiO_2 (Fig. 3 e and f).

As shown in the XRD patterns of the TiO_2-wrapped nanofiber composite catalysts calcined at different temperatures (500, 600, 700, 800, and 900 °C), the transformation from the anatase to rutile phase was accompanied with the carbonization of cellulose. TG-DTA was performed to explore the process of this phase transformation.
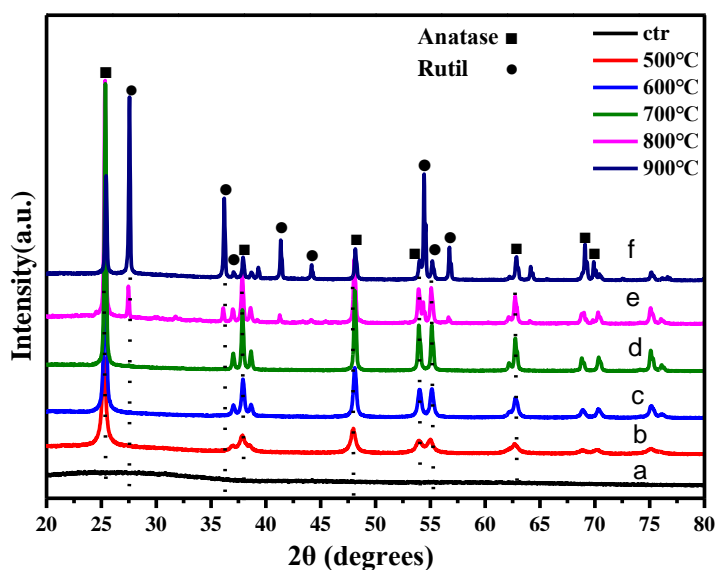

Fig. 5. Typical XRD patterns of the pure sample and samples calcined at different temperatures
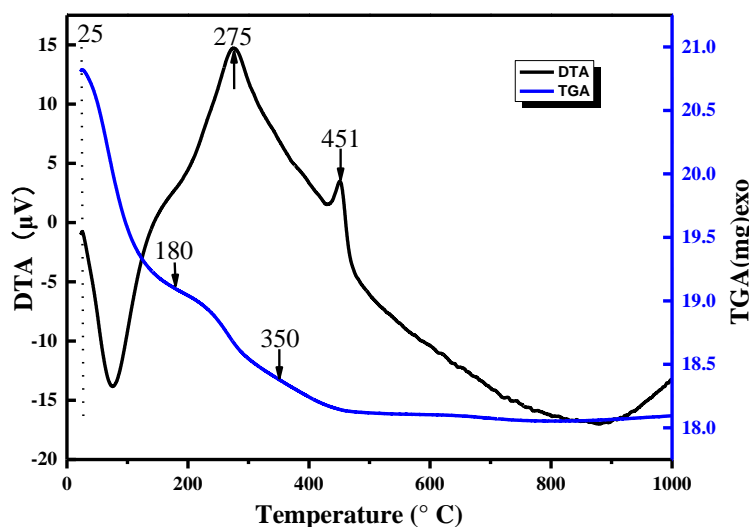
Fig. 6. TG-DTA curves of the TiO₂-wrapped nanofiber hybrid materials

Figure 6 represented the TG-DTA of the TNC composites, including the transformation process of the titania/cotton nanofiber composites to TiO₂-wrapped nanofiber hybrid materials under nitrogen atmosphere. In the TG-DTA curves, the weight loss of the samples was mainly showed in three steps. The first mass loss ranged from about 25 to 180 °C and was attributed to absorbed water, which was determined from the endothermic peak in the DTA curve. The DTA curve showed two exothermic peaks at 275 and 450 °C. The first exothermic peak began at 180 °C and finished at 350 °C, which was assigned to the carbonization process of the cellulose. The results were in accordance with previously reported values (Wielage *et al.* 1999; Moltó *et al.* 2006). The exothermic peak at 450 °C indicated the phase transformation of TiO₂ from the anatase to rutile phase.
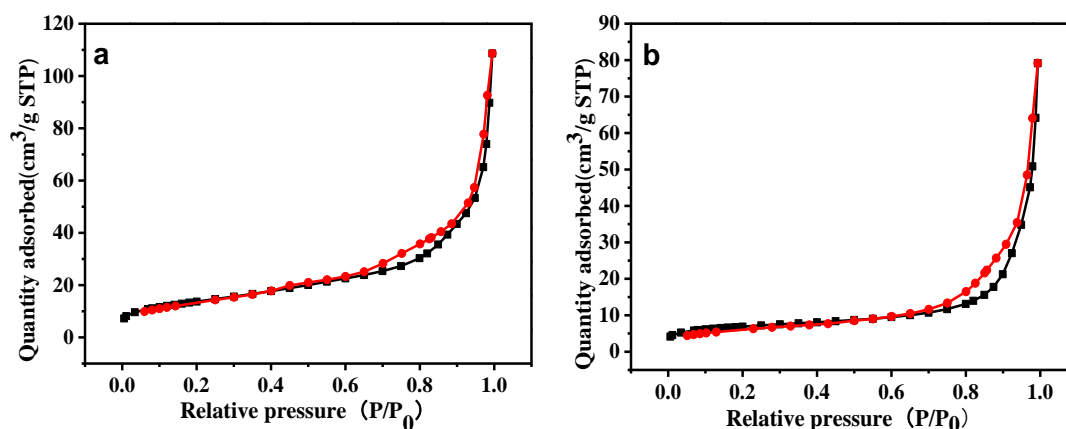

Fig. 7(a & b). N₂ adsorption-desorption isotherms of the TiO₂-wrapped nanofiber hybrid materials after being calcined at (a) 500, (b) 600, (c) 700, (d) 800, and (e) 900 °C

bioresources.com

Fig. 7(c, d, & e). N_2 adsorption-desorption isotherms of the TiO_2-wrapped nanofiber hybrid materials after being calcined at (a) 500, (b) 600, (c) 700, (d) 800, and (e) 900 °C
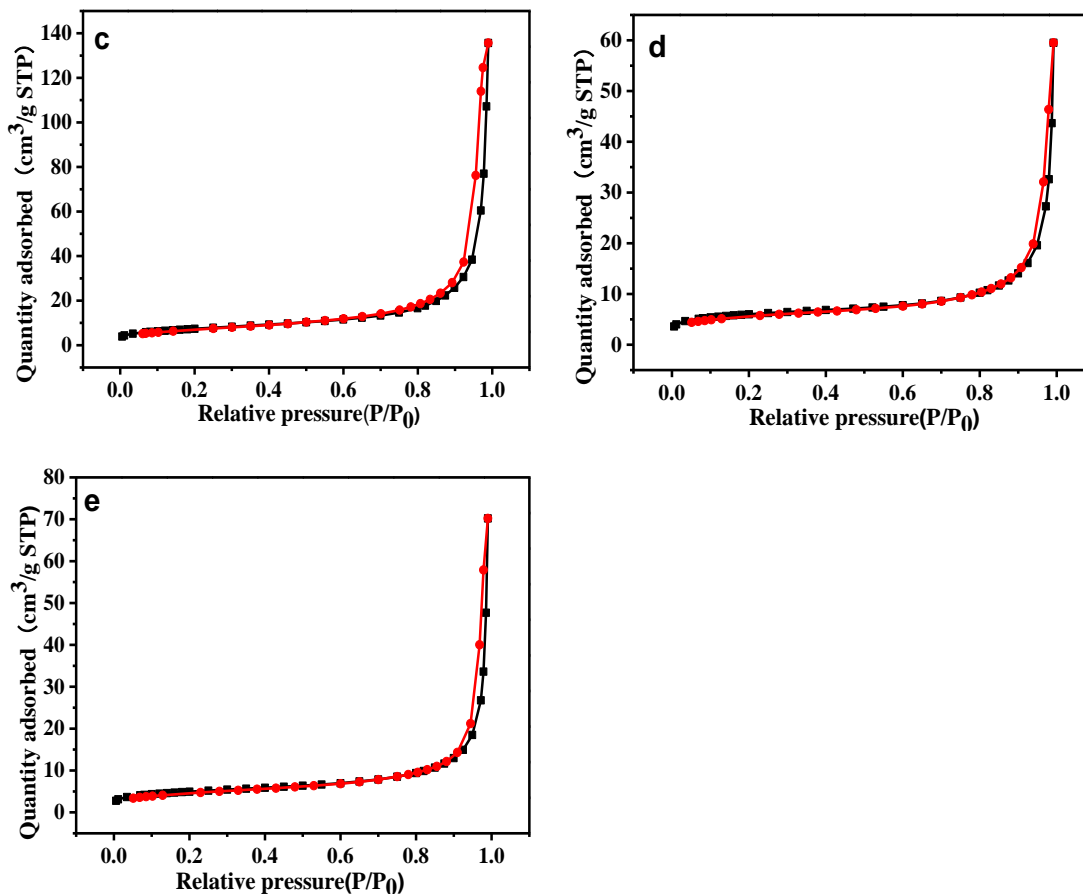
Table 1. Impact of the Calcination Temperature on the BET Specific Surface Area (S_{BET}), Pore Volume (V_p), and Pore Diameter (D) of the TiO_2-Wrapped Nanofiber Hybrid Materials

Sample	S_{BET} (m²/g)	V_p[a] (cm³/g)	Mean D (nm)	
			BET[b]	BJH[c]
TNC	448.4715	0.624687	3.63086	5.9666
TNC-500	48.4650	0.165771	6.89872	12.4796
TNC-600	24.0696	0.122240	9.03679	20.9662
TNC-700	26.0281	0.208321	9.70474	30.8519
TNC-800	21.2634	0.091936	5.75733	22.6055
TNC-900	17.5230	0.108448	6.60419	27.2303

a: BJH adsorption cumulative pore volume of pores between 1.7 and 300 nm in diameter;
b: Adsorption average pore diameter ($4V/A$ by BET); c: BJH desorption average pore diameter ($4V/A$).

BET Analysis of the Composite Catalysts

The BET surface area, pore volumes, and pore sizes of the samples are summarized in Fig. 7 and Table 1. Figure 7 depicted the N_2 adsorption-desorption isotherms of the samples. According to the IUPAC classification, the N_2 isotherm results of all samples were typical of type IV with an H_2-type hysteresis loop, which confirmed that most of the

***bioresources*.com**

pores were mesopores (2 to 50nm). Furthermore, the hysteresis loop was moved to a higher relative pressure range with the rising of the calcination temperature, and simultaneously, the area of the hysteresis loop decreased. The multi-layer adsorption and capillary condensation steps mainly appeared at the high relative pressure range of 0.6 to 0.98, which further established that the relatively massive and uniform mesopores were constituted on the surface of the TiO_2-wrapped nanofiber hybrid materials. Moreover, the results indicated that the samples possessed multifarious roller distributions of porous materials because of the presence of H_2 hysteresis loops, which are observed in the high relative pressure range of 0.6 to 0.98. Compared with the N_2 adsorption-desorption isotherm curves of the other five samples, the TNC-700 sample showed the highest adsorption capacity. As shown in Table 1, the TNC-700 sample had the highest pore volume (0.2083 cm^3/g). That was because of the decrease of pores volumes at higher calcination temperatures. These were due to the destruction of catalyst morphology for the high calcination temperature above 700℃. The structure of rod-like nanofiber composite catalysts could be maintained below 700℃ during the carbonization process of cellulose. This was one of the reason why TNC-800 and TNC-900 showed the relatively poor photocatalytic activities. From Table 1, the surface area, which is one of the most important factors for enhancing the photocatalytic activity, varied as the calcination temperature increased. The BET method was implemented to measure the surface area and porosity of the TiO_2-wrapped nanofiber hybrid materials. The BET specific surface area of the TNC sample was 448.47 m^3/g, and the pore volume was 0.625 cm^3/g.

XPS Analysis of the Composite Catalysts

To characterize the chemical composition and chemical states of the samples at different temperatures, the samples calcined at different temperatures were investigated by XPS analysis (Fig. 8). The TNC-700 samples had a higher binding energy for the C 1s, O 1s, and Ti 2p XPS spectra than the other samples. The results indicated that the strong integration between activated carbon fiber and TiO_2 be calcined at the temperature of 700 °C under nitrogen atmosphere. Results also confirmed the temperature of 700 °C was the optimal choice for fabrication of TiO_2-wrapped nanofiber composite catalysts. By calcination treatment in this temperature, catalysts had the strongest interaction between the Ti, O, and C compared with other samples. Therefore, it also could be understood that the TNC-700 samples showed the fascinating properties for degrading the MB, which is shown in Fig. 10. The peak of C 1s, O 1s, and Ti 2p in the survey spectra of the TNC-700 samples are shown in Fig. 9a. Two intense peaks for Ti $2p_{3/2}$ at 458.6 eV and Ti $2p_{1/2}$ at 464.3 eV are shown in Fig. 9b, and there was a peak separation of 5.7 eV between those two peaks. Liu and Wang (2002). The results both indicated the existence of Ti^{4+} ions (TiO_2). Figure 9c displays the spectra of C 1s, and information of the different carbon-carbon bonding characteristics found from the raw data. Three intense peaks at 284.9, 286.5, and 288.2 eV were observed for the TiO_2-wrapped nanofiber hybrid materials that corresponded to the C 1s binding energy region. Furthermore, the oxygen-containing functional groups, which were affiliated with carbon, showed high peaks for C-O (286.5 eV) and C=O (288.2 eV) at the higher binding energy region. Additionally, the peak at

284.9 eV was assigned to the C-C, C=C, and C-H bonds (sp^2), which was in accordance with other literature (Takahagi and Ishitani 1984; Paiva *et al.* 2000). The O 1s spectra of the TNC-700 hybrid materials are presented in Fig. 9 d. The O 1s region of the samples revealed the existence of two similar peaks corresponding to Ti-O of TiO_2 (530.5 eV) and C-O bonds of carbon fibers (532.5 eV) (Paiva *et al.* 2000; Yu *et al.* 2000; Liu and Wang 2002). This strong evidence confirmed that TiO_2 was successfully loaded on the nanocellulose fiber through chemical bonds. Therefore, the TNC-700 sample displayed higher photocatalytic performance.
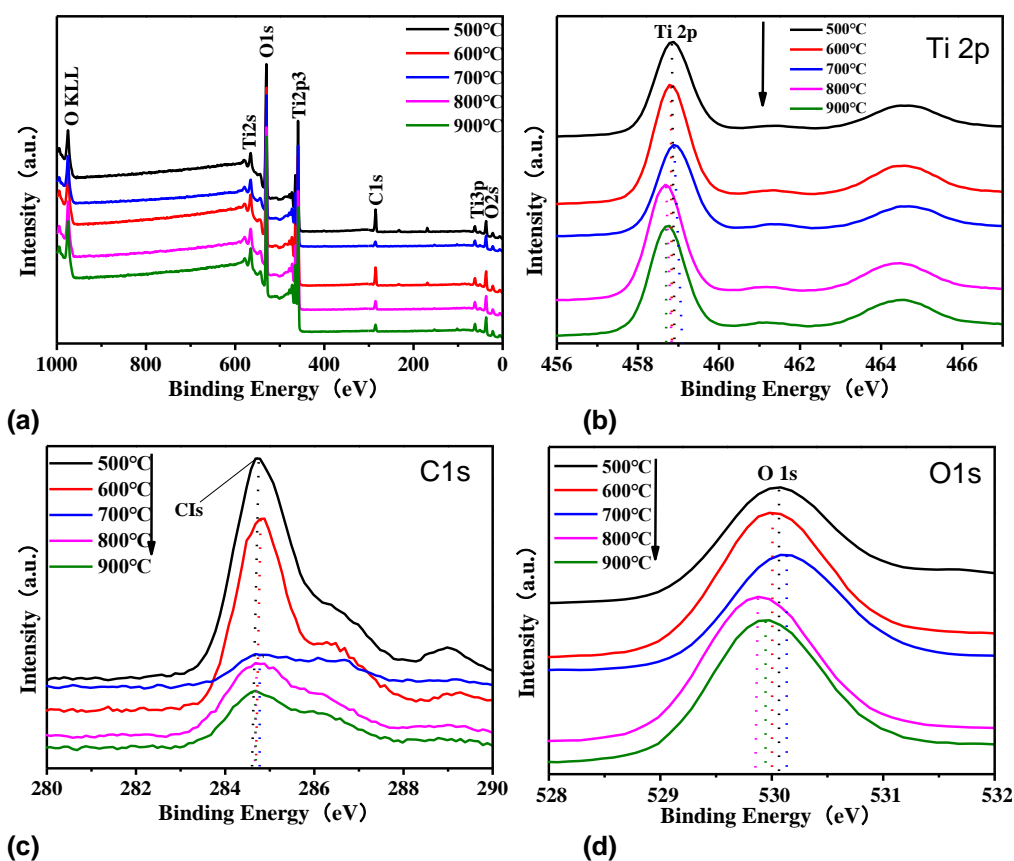
Fig. 8. XPS results of the (a) survey scan spectra and (b) Ti 2p, (c) C 1s, and (d) O 1s regions of the TiO_2-wrapped nanofiber hybrid materials

Photocatalytic Analysis of the Composite Catalysts

Photocatalytic experiments were implemented to investigate the photocatalytic activity of the samples. The catalysts were evaluated by decomposing 10 mg/L MB under UV light irradiation (wavelength = 365 nm, power = 1000 W). MB is a typical organic dye that often contaminates the environment. The dye molecules were quickly adsorbed onto the surface of the catalysts because of the unique porous structure, and then upon decomposition. The blank experiments with no catalysts were conducted under the same conditions in this study.
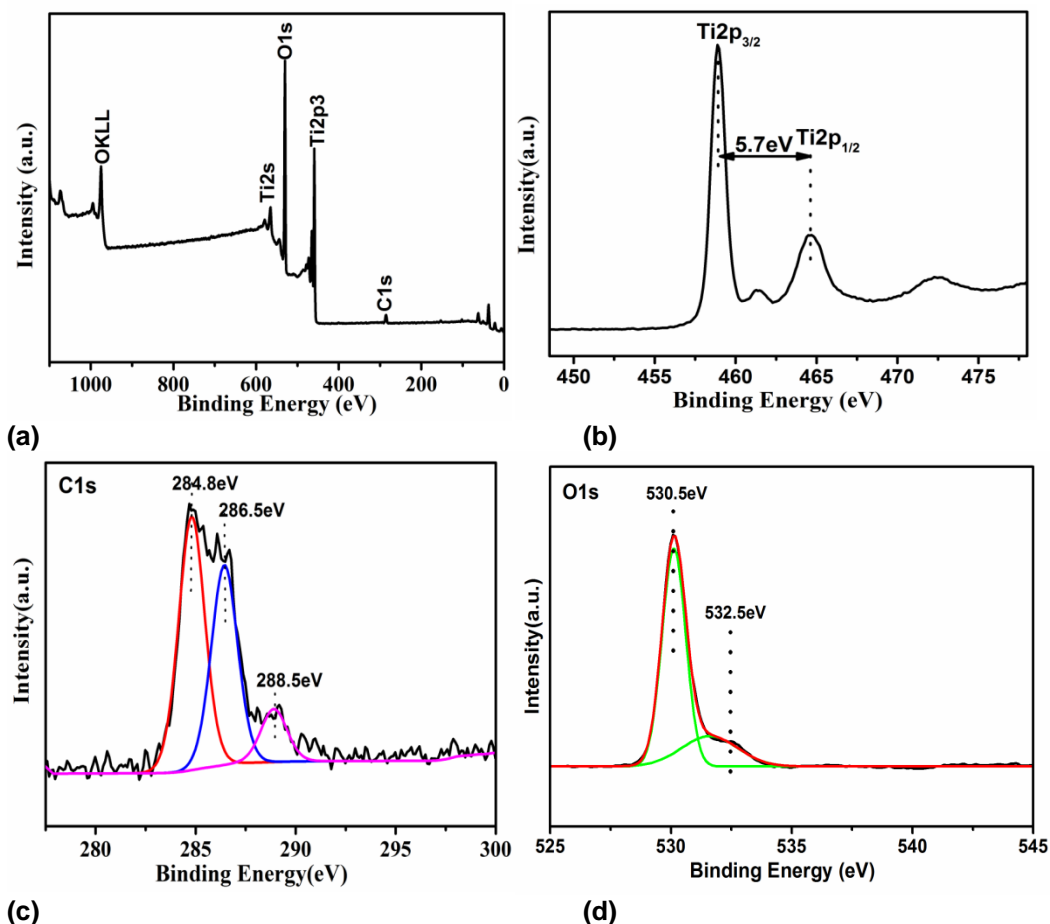
Fig. 9. XPS results for (a) survey scan spectra; (b) Ti 2p; (c) C 1s; (d) O 1s regions for TNC-700

Figure 10 shows that the photodegradation efficiencies of the TNC-500, TNC-600, and TNC-700 samples were beyond that of P25 (TiO_2 nanoparticles). In particular, the photodegradation efficiency of the TNC-700 sample was approximately 35% higher than that of the P25 for the MB solution, while the TNC-800 and TNC-900 samples had relatively poor photocatalytic activities.
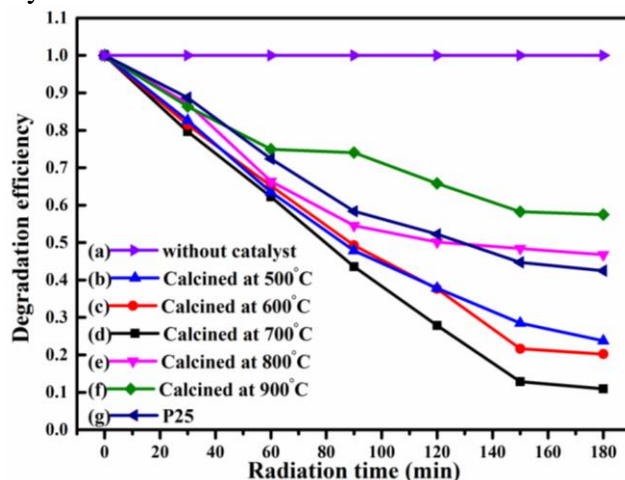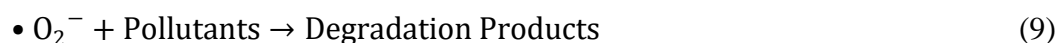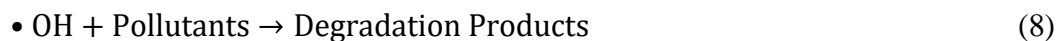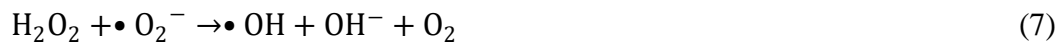

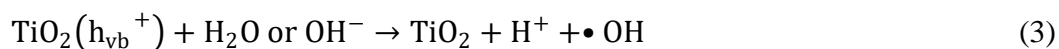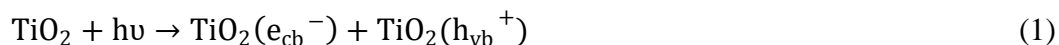**Fig. 10.** Photocatalytic activity of (a) no catalyst, (b) TNC-500, (c) TNC-600, (d) TNC-700, e) TNC-800, (f) TNC-900, and (g) P25

bioresources.com

The discrepancy of the photocatalytic properties between the different samples could be because of the following reasons. First, the BET surface area of these samples played a necessary role in catalytic decomposition, which strongly fluctuated with the different calcination temperatures. The S_{BET} values of the TNC-500 samples were 48.46 m^2/g, which were the highest of all of the samples, and the S_{BET} of the TNC-700 sample was 26.03 m^2/g. The S_{BET} of the samples decreased as the calcination temperature increased above 700 °C. As Table 1 showed, the S_{BET} values of the TNC-800 and TNC-900 samples were 21.26 and 17.52 m^2/g, respectively. The different effect of the photocatalysts could be explained by the discrepancy of the S_{BET} between the five samples. It should be noted that the TNC-700 samples showed the highest photocatalytic degradation rate for MB. However, the S_{BET} values of the TNC-700 samples were the second highest among all of the samples. That was because the TNC-700 sample had a bicrystal phase of anatase and rutile, which was demonstrated in the XRD patterns (Fig. 5). As the calcination temperature increased, the mixed-phase photocatalysts also underwent cellulose carbonization. The difference between the conduction band (CB) edges of the two phases could have facilitated irreversible charge transfer from one phase to the other. The charge transfer contributed to the reduction of the chance for photogenerated electrons and holes recombination. Such as, the TNC-700 samples showed superior photoactivity. Usually, a decrease of the S_{BET} was ascribed to the aggregation of TiO_2 nanoparticles, which was confirmed by the SEM images (Fig. 4). Figure 4 shows that the TNC-700 samples were nanofiber-shaped and had superior dispersion. The TNC-700 samples showed the highest photocatalytic activity, which was due to the appropriate mixed phase of TiO_2, photogenerated electrons quickly transforming from rutile to anatase (rutile antenna mechanism), and efficient electron-hole pairs separation. However, when the calcination temperature was up to 800 and 900 °C, the photocatalytic degradation rate was a little low. The results could be ascribed to the larger percentage of TiO_2 rutile phase and lower S_{BET} of the samples, and further confirmed that the TNC-700 samples possessed a superior photocatalytic activity compared with the other photocatalysts.

The synergistic effect of the TiO_2 and carbon fiber for the TiO_2-wrapped nanofiber hybrid materials contributed to the noticeable enhancement of the photocatalytic activity, as well as its unique structure and properties. The unique porous structure of the TiO_2-wrapped nanofiber hybrid materials had the exclusive advantage of preventing the clustering of TiO_2 nanoparticles, and guaranteed a high specific surface area and strong adsorption capability. Moreover, the hydroxyl groups on the surface of the TiO_2, the existence of which were shown by FTIR spectroscopy, not only improved the adsorption of MB molecules (Anderson and Bard 1997; Ang *et al.* 2009), but also retarded the photogenerated electron-hole pairs recombination process by a hole-trapping effect, and enhanced photocatalytic oxidation. The porous active carbon nanofiber, which acted as a catalyst support, concentrated the target substrate onto its surface, enhanced the adsorption capacity, and provided a substrate-rich environment on the interface of the carbon/TiO_2 nanocrystal composite catalysts. The adsorbed MB molecules were decomposed afterwards.

When the light energy was equal to or greater than the band gap energies (hv), the electrons could be excited from the valence band (VB) to the CB of the catalyst, and the electron-hole pairs (e^-/h^+) of the TiO_2 photocatalyst were generated. The photogenerated positive holes (h^+) reacted with hydroxyl groups (-OH) and/or adsorbed water molecules to generate hydroxyl radicals ($^\bullet OH$), which acted as strong oxidizing agents during the

bioresources.com

photocatalytic reaction, and then the potential hydroxyl radicals (•OH) rapidly reacted with MB. Moreover, the photogenerated electrons (e⁻) reacted with electron acceptors, such as O_2 adsorbed onto the surface of the catalyst or dissolved in water, to produce the superoxide radical anions O_2• and •HO_2. The •OH radicals were also utilized for the oxidation of MB. Additionally, the •HO_2 radicals reacted with each other, resulting in the formation of hydrogen peroxide and increasing the gaseous oxygen in the photocatalytic reaction. Because of the high oxidizing potential of the hydroxyl, superoxide, and •HO_2 radicals, the radicals could react with organic pollutants to produce degradation products. An ordinary simplified scheme of the photocatalytic process was given by Eqs. 1 to 10. Both water and gaseous oxygen played an important part during the photocatalytic reaction, as could be seen by the following equations:

$$TiO_2 + h\upsilon \rightarrow TiO_2(e_{cb}{}^-) + TiO_2(h_{vb}{}^+) \tag{1}$$

$$TiO_2(e_{cb}{}^-) + TiO_2(h_{vb}{}^+) \rightarrow energy \tag{2}$$

$$TiO_2(h_{vb}{}^+) + H_2O \text{ or } OH^- \rightarrow TiO_2 + H^+ +• OH \tag{3}$$

$$TiO_2(e_{cb}{}^-) + O_2 \rightarrow TiO_2 +• O^{2-} \tag{4}$$

$$O_2 + e^- + H^+ \rightarrow• O^{2-} + H^+ \rightarrow• OOH \tag{5}$$

$$2 • HO_2 \rightarrow H_2O_2 + O_2 \tag{6}$$

$$H_2O_2 +• O_2{}^- \rightarrow• OH + OH^- + O_2 \tag{7}$$

$$• OH + Pollutants \rightarrow Degradation \ Products \tag{8}$$

$$• O_2{}^- + Pollutants \rightarrow Degradation \ Products \tag{9}$$

$$HO_2 • +Pollutants \rightarrow Degradation \ Products \tag{10}$$

CONCLUSIONS

1. TiO_2-wrapped nanofiber hybrid materials, which possessed a unique porous structure and mixed crystalline phase, were synthesized by the combination of surface sol–gel and post-calcination processes. By means of the surface sol–gel process, TiO_2 was deposited on the surface of each nanocellulose fiber, and then the TiO_2-wrapped nanofiber hybrid materials were calcined at different temperatures under nitrogen atmosphere.

2. The morphology, crystalline phase, specific surface area, and chemical composition of the novel photocatalysts were characterized by SEM, TEM, XRD, FTIR, TG-DTA, BET, and XPS. With the rising of the calcinations temperature, the original cellulose nanofibers were converted into porous carbon nanofibers, which were wrapped by TiO_2 and accompanied by a crystal transformation.

3. The photocatalytic activity of the new catalysts was evaluated by the degradation of MB under UV irradiation. The results demonstrated that the new catalysts showed better photocatalytic ability, and the photocatalysis degradation effect under UV light irradiation was in the order of TNC-700, TNC-600, TNC-500, P25, TNC-800 and TNC-900 samples from high to low. The TNC-700 catalysts showed a superior photocatalytic ability compared with the other catalysts. The high photocatalytic activity of the TNC-700 samples could be due to the three following crucial factors: the unique appropriate porous structure, high specific surface area and mixed crystalline phase with proper anatase and rutiles. The synergistic photocatalytic effect of the TiO_2 and carbon nanofibers favored the degradation of organic pollutants in water or air.

ACKNOWLEDGMENTS

REFERENCES CITED

Alexandre, M., and Dubois, P. (2000). "Polymer-layered silicate nanocomposites: Preparation, properties and uses of a new class of materials," *Mater. Sci. Eng. R.* 28(1-2), 1-63.DOI:10.1016/S0927-796X(00)00012-7

Alonso, B., and Belamie, E. (2010). "Chitin–silica nanocomposites by self-assembly," *Angew. Chem. Int. Edit.* 49(44), 8201-8204. DOI: 10.1002/anie.201002104

Anderson, C., and Bard, A. J. (1997). "Improved photocatalytic activity and characterization of mixed TiO_2/SiO_2 and TiO_2/Al_2O_3materials," *J. Phys. Chem. B* 101(14), 2611-2616. DOI: 10.1021/jp9626982

Ang, T. P., Toh, C. S., and Han, Y.-F. (2009). "Synthesis, characterization, and activity of visible-light-driven nitrogen-doped TiO_2−SiO_2mixed oxide photocatalysts," *J. Phys. Chem. C* 113(24), 10560-10567. DOI: 10.1021/jp9000658

Ao, Y., Xu, J., Fu, D., and Yuan, C. (2008). "Photoelectrochemical application of hollow titania film," *Electrochem. Commun.* 10(11), 1812-1814. DOI: 10.1016/j.elecom.2008.09.015

Bae, J. Y., Yun, T. K., Han, S. S., Min, B. G., Bako, I., and Suh, S. H. (2009). "Fabrication and characteristics of variable crystalline TiO_2 for photocatalytic activities," *Rev. Roum. Chim.* 54(9), 773-778.

Beck-Candanedo, S., Roman, M., and Gray, D. G. (2005). "Effect of reaction conditions on the properties and behavior of wood cellulose nanocrystal suspensions," *Biomacromolecules* 6(2), 1048-1054. DOI: 10.1021/bm049300p

Bezrodna, T., Puchkovska, G., Shymanovska, V., Baran, J., and Ratajczak, H. (2004). "IR-analysis of H-bonded H_2O on the pure TiO_2," *J. Mol. Struct.* 700(1–3), 175-181. DOI:10.1016/j.molstruc.2003.12.057

Bi, Z., Paranthaman, M. P., Menchhofer, P. A., Dehoff, R. R., Bridges, C. A., Chi, M., Guo, B., Sun, X.-G., and Dai, S. (2013). "Self-organized amorphous TiO_2 nanotube arrays on porous Ti foam for rechargeable lithium and sodium ion batteries," *J. Power Sources* 222, 461-466.DOI: 10.1016/j.jpowsour.2012.09.019

Chen, Y. F., Lee, C. Y., Yeng, M. Y., and Chiu, H. T. (2003). "The effect of calcination temperature on the crystallinity of TiO_2, nanopowders," *J. Cryst. Growth* 247(3–4), 363-370. DOI:10.1016/S0022-0248(02)01938-3

Cook, G., and Timms, P. L. (2003). "Exact replication of biological structures by chemical vapor deposition of silica," *Angew. Chem.* 42(5), 557-559. DOI:10.1002/anie.200390160

de Souza Lima, M. M., and Borsali, R. (2004). "Rodlike cellulose microcrystals: Structure, properties, and applications," *Macromol. Rapid Comm.* 25(7), 771-787. DOI: 10.1002/marc.200300268

Díez, I., Eronen, P., Österberg, M., Linder, M. B., Ikkala, O., and Ras, R. H. A. (2011). "Functionalization of nanofibrillated cellulose with silver nanoclusters: Fluorescence and antibacterial activity," *Macromolecular Bioscience* 11(9), 1185-1191. DOI: 10.1002/mabi.201100099

Eichhorn, S. J., Dufresne, A., Aranguren, M., Marcovich, N. E., Capadona, J. R., Rowan, S. J., Weder, C., Thielemans, W., Roman, M., Renneckar, S., *et al.* (2010)."Review: Current international research into cellulose nanofibres and nanocomposites," *J. Mater. Sci.* 45(1), 1-33. DOI: 10.1007/s10853-009-3874-0

Foo, C. W. P., Patwardhan, S. V., Belton, D. J., Kitchel, B., Anastasiades, D., Huang, J., Naik, R. R., Perry, C. C., and Kaplan, D. L. (2006). "Novel nanocomposites from spider silk-silica fusion (chimeric) proteins," *P. Natl. Acad. Sci. USA* 103(25), 9428-9433. DOI: 10.1073/pnas.0601096103

Gebauer, D., Oliynyk, V., Salajkova, M., Sort, J., Zhou, Q., Bergström, L., and Salazar-Alvarez, G. (2011). "A transparent hybrid of nanocrystalline cellulose and amorphous calcium carbonate nanoparticles," *Nanoscale* 3(9), 3563-3566. DOI: 10.1039/C1NR10681C

Ifuku, S., Morooka, S., Morimoto, M., and Saimoto, H. (2010). "Acetylation of chitin nanofibers and their transparent nanocomposite films," *Biomacromolecules* 11(5), 1326-1330. DOI: 10.1021/bm100109a

Jia, G., Yang, M., Song, Y., You, H., and Zhang, H. (2009). "General and facile method to prepare uniform Y_2O_3: Eu hollow microspheres," *Crystal Growth and Design* 9(1), 301-307. DOI: 10.1021/cg8004823

Jia, N., Li, S.-M., Ma, M.-G., Sun, R.-C., and Zhu, J.-F. (2012). "Hydrothermal fabrication, characterization, and biological activity of cellulose/$CaCO_3$ bionanocomposites," *Carbohyd. Polym.* 88(1), 179-184.DOI: 10.1016/j.carbpol.2011.11.086

Kemell, M., Pore, V., Ritala, M., Leskelä, M., and Lindén, M. (2005). "Atomic layer deposition in nanometer-level replication of cellulosic substances and preparation of photocatalytic TiO_2/cellulose composites," *J. Am. Chem. Soc.* 127(41), 14178-14179.DOI: 10.1021/ja0532887

Kettunen, M., Silvennoinen, R. J., Houbenov, N., Nykänen, A., Ruokolainen, J., Sainio, J., Pore, V., Kemell, M., Ankerfors, M., Lindström, T., *et al.* (2011). "Photoswitchable superabsorbency based on nanocellulose aerogels," *Advanced Functional Materials* 21(3), 510-517. DOI: 10.1002/adfm.201001431

Khan, S. U., Alshahry, M., and Ingler, W. B. Jr. (2002). "Efficient photochemical water splitting by a chemically modified n-TiO_2," *Science* 297(5590), 2243-2245. DOI: 10.1002/chin.200302016

Kharlampieva, E., Kozlovskaya, V., Gunawidjaja, R., Shevchenko, V. V., Vaia, R., Naik, R. R., Kaplan, D. L., and Tsukruk, V. V. (2010)."Flexible silk–inorganic nanocomposites: From transparent to highly reflective," *Advanced Functional Materials* 20(5), 840-846.DOI: 10.1002/adfm.200901774

Klemm, D., Heublein, B., Fink, H.-P., and Bohn, A. (2005)."Cellulose: Fascinating biopolymer and sustainable raw material," *Angew. Chem. Int. Edit.* 44(22), 3358-3393.DOI: 10.1002/anie.200460587

Klemm, D., Kramer, F., Moritz, S., Lindström, T., Ankerfors, M., Gray, D., and Dorris, A. (2011). "Nanocelluloses: A new family of nature-based materials," *Angew. Chem. Int. Edit.* 50(24), 5438-5466. DOI: 10.1002/anie.201001273

Klemm, D., Schumann, D., Kramer, F., Heßler, N., Hornung, M., Schmauder, H. P., and Marsch, S. (2006). "Nanocelluloses as innovative polymers in research and application polysaccharides II," *Adv. Polym. Sci.* 205(1), 49-96.DOI: 10.1007/12_097

Korhonen, J. T., Kettunen, M., Ras, R. H., and Ikkala, O. (2011)."Hydrophobic nanocellulose aerogels as floating, sustainable, reusable, and recyclable oil absorbents," *ACS Applied Materials & Interfaces* 3(6), 1813-1816. DOI: 10.1021/am200475b

Li, W., and Zeng, T. (2011)."Preparation of TiO_2 anatase nanocrystals by $TiCl_4$ hydrolysis with additive H_2SO_4," *Plos One* 6(6), e21082. DOI: 10.1371/journal.pone.0021082

Liu, F. M., and Wang, T. M. (2002). "Surface and optical properties of nanocrystalline anatase titania films grown by radio frequency reactive magnetron sputtering," *App. Surf. Sci.* 195(1–4), 284-290. DOI: 10.1016/S0169-4332(02)00569-X

Liu, G., Zhao, Y., Sun, C., Li, F., Lu, G. Q., and Cheng, H.-M. (2008)."Synergistic effects of B/N doping on the visible-light photocatalytic activity of mesoporous TiO_2," *Angew. Chem. Int. Edit.* 47(24), 4516-4520. DOI: 10.1002/anie.200705633

Marandi, G. B., Kermani, Z. P., and Kurdtabar, M. (2013)."Fast and efficient removal of cationic dyes from aqueous solution by collagen-based hydrogel nanocomposites," *Polym.-Plast. Technol.* 52(3), 310-318.DOI: 10.1080/03602559.2012.748806

Matsui, K. N., Larotonda, F. D. S., Paes, S. S., Luiz, D. B., Pires, A. T. N., and Laurindo, J. B. (2004)."Cassava bagasse-kraft paper composites: Analysis of influence of impregnation with starch acetate on tensile strength and water absorption properties," *Carbohyd. Polym.* 55(3), 237-243.DOI: 10.1016/j.carbpol.2003.07.007

Moltó, J., Font, R., Conesa, J. A., and Martín-Gullón, I. (2006)."Thermogravimetric analysis during the decomposition of cotton fabrics in an inert and air environment," *J. Anal. Appl. Pyrol.* 76(1-2), 124-131. DOI: 10.1016/j.jaap.2005.09.001

Paiva, M. C., Bernardo, C. A., and Nardin, M. (2000). "Mechanical, surface and interfacial characterisation of pitch and pan-based carbon fibres," *Carbon*, 38(9), 1323-1337. DOI: 10.1016/S0008-6223(99)00266-3

Rhim, J.-W., Lee, J.-H., and Hong, S.-I. (2006). "Water resistance and mechanical properties of biopolymer (alginate and soy protein) coated paperboards," *LWT-Food Sci. Technol.* 39(7), 806-813.DOI: 10.1016/j.lwt.2005.05.008

Shanmugasundaram, S., and Horst, K. (2003). "Tageslicht‐Photokatalyse durch Kohlenstoff‐modifiziertes Titandioxid," *Angew. Chem.* 115(40), 5057-5060. DOI: 10.1002/ange.200351577

Sinha Ray, S., and Okamoto, M. (2003)."Polymer/layered silicate nanocomposites: A review from preparation to processing," *Prog. Polym. Sci.* 28(11), 1539-1641. DOI:10.1016/j.progpolymsci.2003.08.002

Stoica-Guzun, A., Stroescu, M., Jinga, S. I., Jipa, I. M., and Dobre, T. (2013). "Microwave assisted synthesis of bacterial cellulose-calcium carbonate composites," *Ind. Crop. Prod.* 50, 414-422. DOI: 10.1016/j.indcrop.2013.07.063

Sun, X., and Li, Y. (2004). "Ga_2O_3 and GaN semiconductor hollow spheres," *Angew. Chem. Int. Edit.* 43(29), 3827-3831. DOI: 10.1002/anie.200353212

Takahagi, T., and Ishitani, A. (1984). "XPS studies by use of the digital difference spectrum technique of functional groups on the surface of carbon fiber," *Carbon* 22(1), 43-46. DOI: 10.1016/0008-6223(84)90131-3

Thakur, V. K., and Thakur, M. K. (2014). "Recent advances in graft copolymerization and applications of chitosan: A review," *ACS Sustain. Chem. Eng.* 2(12), 2637-2652.DOI: 10.1021/sc500634p

Thakur, V. K., and Voicu, S. I. (2016). "Recent advances in cellulose and chitosan based membranes for water purification: A concise review," *Carbohyd. Polym.* 146, 148-165. DOI: 10.1016/j.carbpol.2016.03.030

Watson, S., Beydoun, D., Scott, J., and Amal, R. (2004). "Preparation of nanosized crystalline TiO_2, particles at low temperature for photocatalysis," *J. Nanoparticle Res.* 6(2), 193-207. DOI: 10.1023/B:NANO.0000034623.33083.71

Wielage, B., Lampke, T., Marx, G., Nestler, K., and Starke, D. (1999). "Thermogravimetric and differential scanning calorimetric analysis of natural fibres and polypropylene," *Thermochim. Acta* 337(1-2), 169-177. DOI: 10.1016/S0040-6031(99)00161-6

Yang, Y., and Tian, C. (2015)."Synthesis and characterization of Fe-doped sulfated titania with high photocatalytic activity in visible light," *Res. Chem. Intermediat.* 41(8), 5271-5281. DOI: 10.1007/s11164-014-1628-3

Yu, J., Zhao, X., and Zhao, Q. (2000). "Effect of surface structure on photocatalytic activity of TiO_2, thin films prepared by sol-gel method," *Thin Solid Films* 379(1–2), 7-14. DOI: 10.1016/S0040-6090(00)01542-X

Zhang, J., Xu, Q., Feng, Z., Li, M., and Li, C. (2008)."Importance of the relationship between surface phases and photocatalytic activity of TiO_2," *Angew. Chem.* 120(9), 1790-1973. DOI: 10.1002/ange.200704788

Zhang, Q.-H., Gao, L., and Guo, J.-K. (1999)."Preparation and characterization of nanosized TiO_2 powders from aqueous $TiCl_4$ solution," *Nanostruct. Mater.* 11(8), 1293-1300. DOI: 10.1016/S0965-9773(99)00421-3

Zhang, Q., Gao, L., and Guo, J. (2000)."Effect of hydrolysis conditions on morphology and crystallization of nanosized TiO$_2$ powder," *J. Eur. Ceram. Soc.* 20(12), 2153-2158. DOI: 10.1016/S0955-2219(00)00085-6

Zhu, G.-X., Wei, X.-W., Xia, C.-J., and Ye, Y. (2007)."Solution route to single crystalline dendritic cobalt nanostructures coated with carbon shells," *Carbon* 45(6), 1160-1166. DOI: 10.1016/j.carbon.2007.02.028